BIOCHEMISTRY
including biophysical chemistry & molecular biology
Article

Biochemistry **2009,** *48,* 5669–5678 5669
DOI: 10.1021/bi900183r

A Rate-Limiting Conformational Step in the Catalytic Pathway of the *glmS* Ribozyme[†]

Krista M. Brooks and Ken J. Hampel*

Department of Microbiology and Molecular Genetics, The Markey Center for Molecular Genetics, Stafford Hall, 95 Carrigan Drive, University of Vermont, Burlington, Vermont 05401

Received February 4, 2009; Revised Manuscript Received May 13, 2009

ABSTRACT: The *glmS* ribozyme is a conserved riboswitch in numerous Gram-positive bacteria and is located upstream of the glucosamine-6-phosphate (GlcN6P) synthetase reading frame. Binding of GlcN6P activates site-specific self-cleavage of the *glmS* mRNA, resulting in the downregulation of *glmS* gene expression. Unlike other riboswitches, the *glmS* ribozyme does not undergo structural rearrangement upon metabolite binding, indicating that the metabolite binding pocket is preformed in the absence of ligand. This observation led us to test if individual steps in the reaction pathway could be dissected by initiating the cleavage reaction before or after Mg^{2+}-dependent folding. Here we show that self-cleavage reactions initiated with simultaneous addition of Mg^{2+} and GlcN6P are slow (3 min^{-1}) compared to reactions initiated by addition of GlcN6P to *glmS* RNA that has been prefolded in Mg^{2+}-containing buffer (72 min^{-1}). These data indicate that some level of Mg^{2+}-dependent folding is rate-limiting for catalysis. Reactions initiated by addition of GlcN6P to the prefolded ribozyme also resulted in a 30-fold increase in the apparent ligand K_d compared to those of reactions initiated by a global folding step. Time-resolved hydroxyl-radical footprinting was employed to determine if global tertiary structure formation is the rate-limiting step. The results of these experiments provided evidence for fast and largely concerted folding of the global tertiary structure (>13 min^{-1}). This indicates that the rate-limiting step that we have identified either is a slow folding step between the fast initial folding and ligand binding events or represents the rate of escape from a nativelike folding trap.

Riboswitches are structural RNA elements present in the untranslated regions of the transcripts they regulate (*1*−*5*). They possess the capacity to control gene expression directly through binding specific metabolites. The *glmS* ribozyme is a conserved element in numerous Gram-positive bacteria and is located upstream of the gene encoding the enzyme glucosamine-6-phosphate (GlcN6P)[1] synthetase, which catalyzes the conversion of glutamine and fructose 6-phosphate to GlcN6P, a metabolic precursor in bacterial cell wall biosynthesis (*6*, *7*). Binding of GlcN6P activates the downregulation of gene expression by inducing self-cleavage of the *glmS* mRNA. This cleavage event initiates rapid degradation of the 3′ cleavage product, including the coding region, by RNase J1 (*8*). The *glmS* ribozyme is unique from other riboswitches in that it does not undergo a conformational rearrangement in the presence of GlcN6P. Previous work has shown that the ligand binding pocket is formed and poised for catalysis in the absence of ligand (*5*, *9*−*12*). This suggests that the role of GlcN6P is strictly chemical in nature and is only required for catalysis, as addition of the metabolite has been shown to increase the cleavage rate 10^5-fold over that of background hydrolysis (*13*).

Strong evidence points toward GlcN6P having a direct function as a coenzyme in the RNA cleavage reaction mechanism, with the amino group being the determining factor of cleavage activity (*11*−*13*). Structural evidence places the ligand in contact with a group of conserved residues near the active site of the ribozyme (*11*, *12*, *14*). Biochemical evidence supporting this role has been obtained using GlcN6P analogues. For example, glucose 6-phosphate (Glc6P), which has a hydroxyl in place of the amine group in GlcN6P, is a competitive inhibitor of the *glmS* ribozyme self-cleavage reaction (*13*). Glucosamine (GlcN) which retains the amine group but lacks the phosphate moiety is able to promote reaction chemistry but at a reduced rate compared to that of GlcN6P (*13*). Soukup and co-workers have demonstrated that the amino pK_a values of GlcN6P and other functional ligand analogues that contain a primary amine (Tris and serinol) affect the cleavage kinetics of the ribozyme (*13*). However, this pH reactivity profile was studied at subsaturating concentrations of GlcN6P (10 μM) and with 10 mM analogue ligands. The resulting pH profile found the cleavage rate to be highly pH dependent, varying broadly (~50-fold) over the pH range studied (5.5−10.0) (*13*). When the pH profile was determined at a saturating concentration of ligand (10 mM GlcN6P), the reaction

[†]K.M.B. was supported by Cancer Biology Training Grant CA09286/22-26 from the National Cancer Institute.

*To whom correspondence should be addressed. E-mail: khampel@uvm.edu. Phone: (802) 656-8507. Fax: (802) 656-8749.

[1]Abbreviations: EDTA, ethylenediaminetetraacetic acid; GlcN6P, glucosamine 6-phosphate; HEPES, *N*-(2-hydroxyethyl)piperazine-*N*′-2-ethanesulfonic acid; HPLC, high-performance liquid chromatography; mRNA, messenger ribonucleic acid; PAGE, polyacrylamide gel electrophoresis; PCR, polymerase chain reaction; TAPS, *N*-tris (hydroxymethyl)methyl-3-aminopropanesulfonic acid; Tris, tris(hydroxymethyl)aminomethane; tRNA, transfer ribonucleic acid; UV, ultraviolet; VS, Varkud satellite.

Published on Web 05/18/2009

rate changed <2-fold over the pH range examined (6.5−9.0), while the apparent K_m of the ligand exhibited a strong pH dependence with the lowest apparent K_m values observed at or above neutral pH (*12*). Clouding the interpretation of these and other data in the field is a lack of clear definition of the rate-limiting step in catalysis under specific reaction conditions. For example, if folding were rate-limiting at the apparent GlcN6P saturation, then the actual rate of coenzyme-mediated catalysis could be much higher than that observed in these studies.

In this study, we find that in vitro, folding of the *glmS* ribozyme into a native, catalytically active form is slow and rate-limiting. To improve our understanding of the chemical mechanism of RNA cleavage and elucidate the role of GlcN6P, we have developed two distinct experimental designs that allow us to dissect the catalytic pathway and determine the individual reaction rates specific to either (1) Mg^{2+}-dependent folding or (2) ligand binding and catalysis.

MATERIALS AND METHODS

RNA Preparation. The short substrate RNA was generated on an Applied Biosystems DNA/RNA synthesizer using standard phosphoramidite chemistry from Glen Research. The RNA products were deprotected and purified by denaturing PAGE and reverse phase HPLC as described previously (*15*). The *glmS*-Rz, cis-*glmS*, and *glmS* 3′P RNAs were made by transcription of double-stranded DNA templates with T7 RNA polymerase. Transcription templates were constructed by annealing two large overlapping DNAs and filling in the single-stranded regions with T4 DNA polymerase and subsequent PCR amplification as previously described (*10*). To generate *glmS*-3′P cleavage products, we added 10 mM GlcN6P to *glmS*-cis transcriptions following the standard transcription incubation of 3 h, and this mixture was allowed to incubate for an additional 1 h at 37 °C. All transcription and cleavage products were purified by polyacrylamide gel electrophoresis as described previously (*16*). Radiolabeled RNAs were prepared by phosphorylation of the 5′-terminal hydroxyl group with [γ-^{32}P]ATP (ICN) and polynucleotide kinase.

Ribozyme Cleavage Kinetics. A buffer (25 mM each) containing TAPS, HEPES, cacodylate, and sodium acetate (THCA) (pH 7.5) was used at all pH values so that buffer-specific effects could be minimized. THCA was pH adjusted by adding NaOH to each buffer stock. The final concentration of Na^+ ions was, therefore, different at each pH. This difference was adjusted by the addition of NaCl to reaction buffers above pH 6 so that the final concentration of Na^+ was equal to 60 mM for all reactions. GlcN6P stocks were adjusted to the pH of the reaction to which they were added.

All RNAs were subjected to a 2 min incubation at 70 °C in 25 mM THCA with 0.1 mM EDTA followed by a 5 min benchtop cooling time. This incubation served to release the RNAs from any nonproductive conformations present upon thawing. The final concentration of *glmS*-Rz was 0.5 μM in all trans reactions. Labeled substrate or cis-cleaving *glmS* constructs were present at <10 nM. RNAs were incubated in 25 mM THCA with or without 15 mM Mg^{2+} and a specified concentration of GlcN6P at 25 °C for 1.5 h. Cleavage reactions were initiated by adding an equal volume of a solution containing 25 mM THCA and specified concentrations of *glmS*-Rz, Mg^{2+}, and GlcN6P. Reactions were quenched by adding 1 μL of the reaction mixture to 9 μL of loading buffer, 95% (v/v) formamide, 25 mM EDTA, 0.01% (w/v) bromophenol blue, and 0.01% (w/v) xylene cyanol. The reaction products were separated on denaturing polyacrylamide gels, 20% acrylamide for trans cleavage reactions and 6% for *glmS*-cis reactions, and the data were quantified using Bio-Rad phosphorimager analysis and Quantity One 1-D software. The resulting data points were plotted and fitted using Synergy's Kalidegraph (version 3.6) according to the double-exponential equation $y = y_o = A_1(1 - e^{-t/\tau_1}) + A_2(1 - e^{-t/\tau_1})$, yielding cleavage rate constants k_i ($=1/\tau_1$) and amplitudes A_i. All experiments were performed a minimum of two times.

Rapid quench reactions were conducted on a three-syringe Kintek rapid quench mixer. Equal volumes from the two sample ports containing RNA and buffer components as described were pushed into the mixing chamber to initiate reactions. The push buffers were identical in composition to the samples that they pushed without the RNA and GlcN6P. The quench syringe contained 86% (v/v) formamide, 35 mM EDTA, and 1× TBE.

Rapid Quench Time-Resolved Hydroxyl-Radical Probing. These reactions were conducted according to the method described previously (*17*). Our reactions were conducted on a three-syringe Kintek rapid quench mixer. The right sample syringe contained 5′-end-labeled *glmS*-3′P in 25 mM cacodylate (pH 7) and 0.1 mM EDTA with or without 15 mM GlcN6P. The left sample syringe contained the folding cation solution, 30 mM Mg^{2+}, and 1.2% (v/v) H_2O_2 with or without 15 mM GlcN6P. Buffer syringes each contained 25 mM cacodylate, with the right and left additionally containing 0.1 mM EDTA and 30 mM Mg^{2+}, respectively. The quench syringe contained 3.25 mM Fe(II) [$Fe(NH_4)_2(SO_4)_2$] and 3.5 mM Na_2-EDTA made up immediately prior to the experiment. Individual reactions proceeded with an initial mixing of equal volumes of the two sample syringes. This mixture was allowed to fold for a specified time at 25 °C prior to rapid mixing with quench. When the quench solution encounters the H_2O_2 within the reaction, a rapid burst of OH radicals is generated which results in rapid cleavage of the RNA backbone. This solution is pushed into a microfuge tube containing 400 μL of ethanol placed at the end of the exit tubing which rapidly and effectively quenches the free radicals in solution. Samples were precipitated in the ethanol solution with the addition of 25 μg of tRNA as a carrier RNA and 0.3 M sodium acetate (pH 7) at −20 °C and collected by centrifugation. Sample pellets were washed with ice-cold 70% ethanol, dried, and resuspended in formamide gel loading buffer. Samples were then separated on denaturing polyacrylamide sequencing gels and analyzed with a Bio-Rad phosphorimager.

Quench flow mixing was used to conduct experiments with folding times from 0.01 to 60 s in Mg^{2+}, and aliquots were run on gels next to several critical control samples. First, two control lanes were included for nonspecific RNA degradation that occurs in the rapid quench machine and the RNA workup. This was accomplished by replacing the quench solution with H_2O and exposing each sample for a 10 s mixing time. A second set of two control samples was included to provide a negative control for tertiary folding where the samples are probed in the absence of Mg^{2+}. Finally, four control lanes were included in which the RNA sample port contains RNA that has been folded in Mg^{2+} for the maximum folding time used in our experiments, 90 min.

Hand-Sampled Hydroxyl-Radical Footprinting Reactions. Folding time points between 60 s and 90 min were taken according to a method that we developed previously (*18*). The samples from these experiments were separated on gels separate from the quench flow samples, but using the same array of controls for nonspecific RNA degradation, the prefolded state of

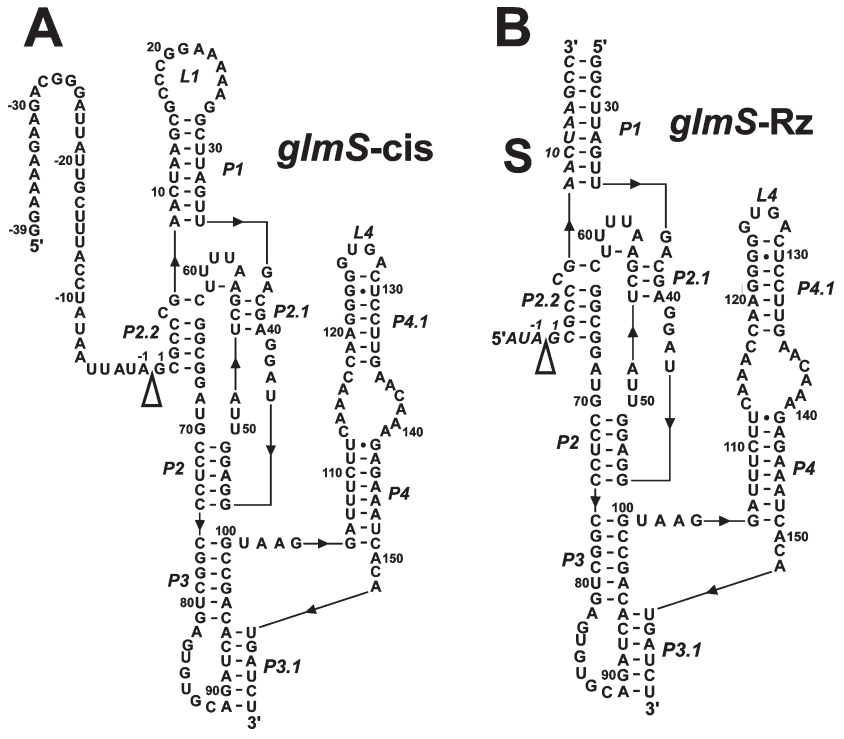

FIGURE 1: Secondary structure diagrams of the *Bacillus subtilis* self-cleaving *glmS* motif (*glmS*-cis) (A) and the *glmS* ribozyme−substrate complex (*glmS*-Rz−S) (B) used in cleavage kinetics experiments. The secondary structures are depicted according to the existing crystal structures for the *glmS* ribozyme (*11*, *12*), and the numbering is according to Winkler and co-workers (*7*). The 5′ to 3′ direction of the RNA is indicated with black triangles. The cleavage site is indicated with a white triangle.

the RNA in the absence of Mg^{2+}, and the final equilibrium folding of the RNA. Quantification of each protected site was carried out by phosphorimager analysis using a Bio-Rad phosphorimaging system. Shcherbakova and Brenowitz have described the quantification procedure in great detail (*17*). Protected fractions at each site were normalized to the highest level of protection observed in individual experiments and plotted as a function of folding time. These plots were fit to the triple-exponential formula $y = y_o + A_1(1 - e^{-t/\tau_1}) + A_2(1 - e^{-t/\tau_1}) + A_3(1 - e^{-t/\tau_1})$ to yield folding rates and magnitudes for each protected site on the *glmS*-3′P. Magnitudes of protection matched our previously reported range (*10*).

RESULTS

Our previous studies indicated that ribozyme−GlcN6P binding does not affect the formation of the native RNA tertiary structure and that a preformed ligand binding pocket is constructed upon incubation with Mg^{2+} (*10*). To test this hypothesis further, we determined the rate of the cleavage reaction under two different experimental designs aimed at partitioning the reaction pathway. In our previous experiments, initiation of cleavage reactions by adding Mg^{2+} to a mixture of ribozyme-bound substrate and GlcN6P resulted in catalysis with a rate of $\sim$4 min^{-1} (*10*). If Mg^{2+}-dependent folding is independent of the ligand binding step, we reasoned that initiating the reaction by adding GlcN6P to a ribozyme prefolded in Mg^{2+} would yield a distinct reaction rate, and perhaps a better approximation of the intrinsic ligand binding rate. A *glmS* mRNA fragment that contains the entire conserved ribozyme sequence required for optimal activity [*glmS*-cis (Figure 1A)] was preincubated in the presence (GlcN6P-initiated) or absence (cation-initiated) of Mg^{2+} and then the reaction initiated by the addition of the complete reaction buffer (Figure 2A,B). The preincubation conditions did not result in any detectable self-cleavage after 90 min in our buffer system (data not shown). We observed that *glmS*-cis molecules that were allowed to prefold in the presence of Mg^{2+} for 90 min self-cleaved very rapidly (72 min^{-1}) compared to reactions initiated from an unfolded state [2.6 min^{-1} (Figure 2B and Table 1)]. The clearest interpretation of this finding is that Mg^{2+}-dependent folding is rate-limiting under conditions where the reactions are initiated by adding Mg^{2+} and ligand to unfolded mRNA. This step has already taken place when the *glmS*-cis construct is allowed to fold for an extended period in Mg^{2+}. It should be noted that we chose a prefolding time of 90 min since in previous equilibrium folding experiments we found no change in the folded fraction beyond that time point under similar reaction conditions (*10*). Likewise, when cleavage reactions are initiated by the addition of Mg^{2+}, the reaction has progressed to a final equilibrium state prior to 90 min (Figure 2B).

Cleavage kinetics experiments were also conducted using these two experimental designs on a trans construct. This allowed us to employ an additional method in which ribozyme and substrate are combined to initiate the reaction [complex-initiated (Figure 2A)]. If a conformational step is rate-limiting for the cleavage reaction, we expect that initiating reactions by adding ribozyme and substrate together would result in a slow rate, similar to that obtained by initiating the reaction by adding a folding cation such as Mg^{2+}. Our previous hydroxyl-radical footprinting data have shown that incubation of the ribozyme−substrate complex or cis-cleaving riboswitch in the absence of Mg^{2+} does not result in solvent protection of the backbone; thus, global tertiary structure is absent (*10*). Two previous investigations have used this type of reaction initiation and observed reactions rates of < 6 min^{-1} (*9*, *12*). Using the complex-initiated method, the rate of catalysis was 3.5 min^{-1} compared to 75 min^{-1} using GlcN6P initiation, indicating that a slow conformational

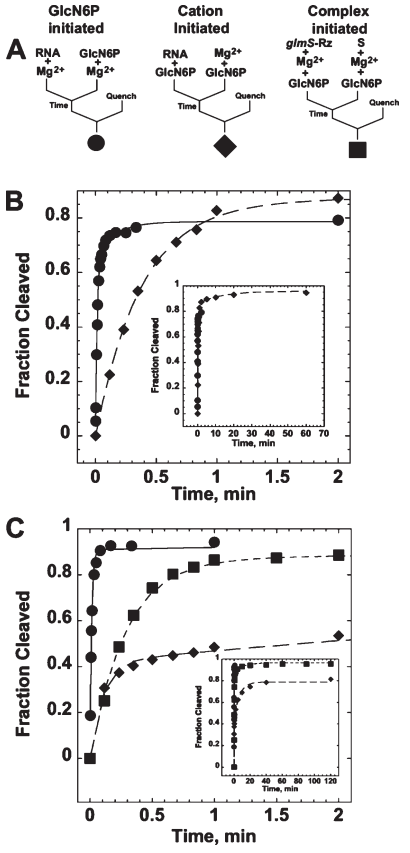

FIGURE 2: Experimental design for the *glmS* ribozyme reactions that affect the cleavage rate. Cleavage assays were conducted according to the three distinct experimental designs shown in panel A: in 25 mM THCA buffer (pH 7.5), 15 mM Mg^{2+}, and 10 mM GlcN6P at 25 °C. Representative plots of the fraction cleaved as a function of time for *glmS*-cis (B) and *glmS*-Rz (C) are shown. Each experiment was completed in triplicate. The standard errors between replicate experiments are given in Table 1. The symbols used in panels B and C are shown below each experimental design in panel A. The insets show the final magnitude of cleavage for each experimental design and construct. Curve fits were calculated by fitting to a double-exponential equation as described in Materials and Methods.

Table 1: Cleavage Rates and Amplitudes for *glmS*-cis and *glmS*-Rz−S Constructs under Various Experimental Designs

construct (experimental design[a])	k_{obs}, fast[b] (min^{-1})	amplitude, fast	k_{obs}, slow (min^{-1})	amplitude, slow
glmS-cis (GlcN6P)	72 ± 3.8	0.66	6.2 ± 2.2	0.13
glmS-cis (cation)	2.6 ± 0.05	0.86	0.08	0.1
glmS-Rz−S (GlcN6P)	75 ± 3.5	0.91	NA	NA
glmS-Rz−S (cation)	9.9 ± 1.2	0.42	0.15 ± 0.02	0.37
glmS-Rz−S (complex)	3.5 ± 0.1	0.86	0.1	0.1

[a] See Figure 2A for the definitions of the GlcN6P-initiated, cation-initiated, and complex-initiated reactions. [b] The fast and slow reaction phases were determined by fitting to double-exponential equations as described in Materials and Methods.

step is rate-limiting (Figure 2C). Cation initiation with the *glmS*-Rz−S complex resulted in a strongly biphasic reaction coordinate, with the fast rate (9.9 min^{-1}) accounting for 42% of the final magnitude of the reaction.

Once we had been able to dissect the reaction pathway, we wanted to explore the individual characteristics of these isolated reaction steps further. The pH dependence of the cleavage reaction is of great interest since clear candidates for chemical constituents at the active site have been hypothesized on the basis

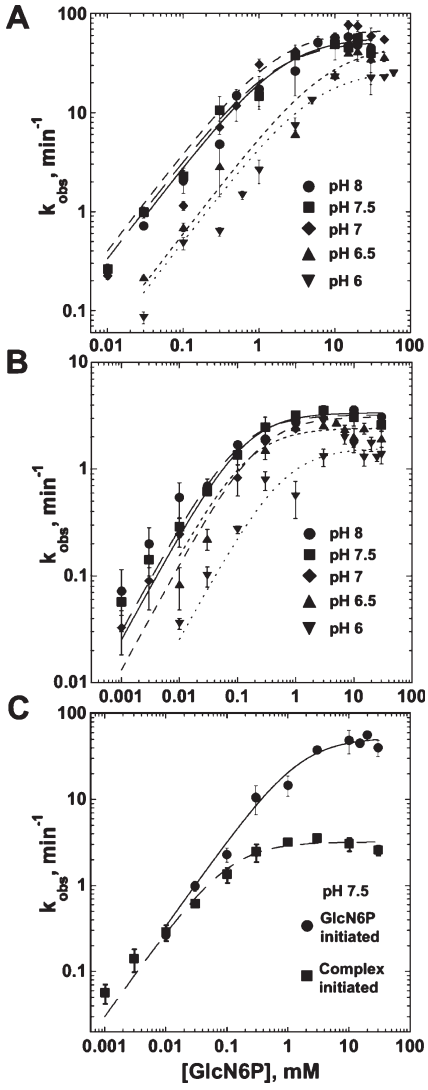

FIGURE 3: Shallow pH dependence of the cleavage rate using GlcN6P-initiated (A) and complex-initiated (B) experimental designs. Reaction rates for the *glmS*-Rz−S complex were plotted as a function of GlcN6P concentration under the GlcN6P-initiated (A) and complex-initiated (B) designs shown in Figure 2 at pH 6−8. The symbols used for each pH are shown in the graphs. Data from panels A and B were replotted (C) to show the GlcN6P dependence of the cleavage reaction as a function of the experimental design employed at pH 7.5. Black circles and diamonds represent data for the GlcN6P-initiated and complex-initiated reactions, respectively. All data points are the average of at least two replicate experiments. The data were fit to the Hill equation assuming $n = 1$ as described in Materials and Methods.

of biochemical and structural data (*11*, *12*, *14*, *19*). Previous pH titrations showed little change in the cleavage rate as a function of pH but demonstrated significant variation of pH-dependent apparent binding constants for GlcN6P (*12*). These experiments utilized an experimental design similar to our complex-initiated trans cleavage reactions (Figure 2A,C), a method that likely makes folding rate-limiting at saturating concentrations of GlcN6P. We carried out ligand titrations over a pH range from 6 to 8. For reactions using both the complex initiation and GlcN6P initiation designs, cleavage rates increased 2−3-fold with an increase in pH (Figure 3 and Table 2). We did, however, observe a significant change in the apparent K_d for GlcN6P between the separate reaction designs. Complex-initiated reactions resulted in an apparent K_d for GlcN6P at pH 7.5 of 0.11 mM, while those performed according to a GlcN6P-initiated

Table 2: Apparent K_d Values for GlcN6P and Maximum Cleavage Rates as a Function of pH for the *glmS*-Rz−S Complex

	complex-initiated[a]		GlcN6P-initiated	
pH	K_d[b] (mM)	k_{obs}^{max} (min^{-1})	K_d (mM)	k_{obs}^{max} (min^{-1})
6	0.61 ± 0.33	1.6 ± 0.13	5.3 ± 1.4	27 ± 1.8
6.5	0.15 ± 0.07	2.4 ± 0.14	8.0 ± 4.5	49 ± 8.3
7	0.23 ± 0.05	3.1 ± 0.13	1.7 ± 0.66	69 ± 5.3
7.5	0.11 ± 0.03	3.2 ± 0.17	1.5 ± 0.56	52 ± 3.7
8	0.13 ± 0.04	3.4 ± 0.17	2.0 ± 0.74	58 ± 4.9

[a] Complex- and GlcN6P-initiated experimental designs are defined in Figure 2 and described in Materials and Methods. [b] K_d values were determined by fitting k_{obs} vs GlcN6P concentration plots to the Hill equation, where the value for the Hill coefficient (n) equals 1, as described in Materials and Methods.

design result in a 26-fold higher apparent K_d [K_d = 2.9 mM (Figure 3C and Table 2)]. When titrations for the two reaction designs are plotted together at a single pH, we see that at low GlcN6P concentrations, the rate of catalysis is identical for both designs, indicating that the GlcN6P binding rate limits the reaction rate (Figure 3C and Figure S1 of the Supporting Information). We know that a change in the rate-limiting step exists in the complex-initiated reaction GlcN6P isotherms so that above a certain GlcN6P concentration no further increase in rate is possible because a slow Mg^{2+}-dependent conformational step becomes rate-limiting. However, in reactions where this step has been completed by prefolding the complex in Mg^{2+} (GlcN6P-initiated), the reaction rate continues to increase with GlcN6P concentration to the point where either the ligand binding rate is saturated or another step in the reaction pathway becomes rate-limiting. Thus, the two different reaction designs give distinct apparent binding constants for GlcN6P.

Since we had evidence for a slow Mg^{2+}-dependent folding step, we wanted to determine if the formation of a global tertiary structure as monitored by hydroxyl-radical footprinting represents this slow step. Previous hydroxyl-radical footprinting experiments have shown a significant solvent protection of the ribozyme−substrate complex in Mg^{2+}-containing solutions (*10*). The positions of solvent-protected sites within the *glmS* ribozyme−substrate complex fit well with the three-dimensional structures determined by X-ray crystallography (*11*, *12*). Folding as fast as 20 s^{-1} should be readily observable in time-resolved footprinting experiments, and we believed that it would be possible to identify intermediates in the folding pathway. These experiments were performed using a method for rapid generation of hydroxyl radicals in the folding solution and quenching as developed by the Brenowitz lab in conjunction with a hand-held time-resolved method developed in our previous studies of the hairpin ribozyme (*17*, *18*). The end-labeled 3′ product of the *glmS*-cis self-cleavage was employed to monitor global folding. This fragment is observed to bind coenzyme in crystal structures (*11*).

In these experiments, equal volumes of 5′-end-labeled *glmS*-3′P in a buffer containing a low concentration of EDTA (0.1 mM) and a buffer containing 30 mM Mg^{2+} and H_2O_2 are rapidly mixed. After a predetermined folding time at a final Mg^{2+} concentration of 15 mM, the folding reaction solution is mixed with a solution containing Fe(II)-EDTA. H_2O_2 included in the Mg^{2+} buffer oxidizes the Fe(II). This reaction generates hydroxyl radicals that cleave the RNA backbone at solvent-exposed ribose residues. The magnitude of solvent protection compared to that of negative folding controls exposed to hydroxyl radicals after incubation in the absence of Mg^{2+} can be determined by phosphorimager analysis of sequencing gels [Figure 4 (*17*, *18*)]. In this manner, we are able to monitor the formation of solvent-protected sites as a function of folding time. We found very fast folding for all solvent-protected sites on the ribozyme and substrate. The folding progress curves for all protected residues display multiphasic behavior and are best fit to a triple-exponential equation. The rates and amplitudes of the two fastest rates are consistent between all protected sites. The fastest rate for folding of each site varied 4-fold and ranged from 3.6 to 14.2 s^{-1}. The second fastest rate ranged from 0.23 to 1.1 s^{-1} (Figure 5). These two faster rates account for 57−78% of the total protection quantified at each site. The slowest of the three rates is poorly defined in our experiments and differs between specific sites by approximately 100-fold. In addition, we did not find a large difference between the folding rates in the presence or absence of GlcN6P, indicating that under these ionic conditions, binding of ligand to the ribozyme does not influence the rate of global tertiary folding (Figure 6). These data complement our RNA cleavage kinetics demonstrating that GlcN6P does not bind to the ribozyme prior to final assembly of the ligand binding domain.

DISCUSSION

In our earlier work, we presented evidence of a preordered ligand binding pocket formed by the addition of divalent cations to the RNA (*10*). This result was supported by crystal structures which showed that the riboswitch in its unbound form has a nearly identical GlcN6P binding structure as when it is bound by GlcN6P or a competitive inhibitor, glucose 6-phosphate (*11*, *12*). In contrast to other riboswitches that use the ligand-dependent conformational changes to effect gene regulation, the *glmS* ribozyme forms the ligand binding pocket in the absence of ligand. Our initial model for the reaction pathway of the ribozyme, therefore, featured apo-riboswitch in equilibrium between a ligand binding mode and an unfolded form. When the RNA is in its ligand binding mode, GlcN6P is able to bind and stimulate RNA self-cleavage (*10*).

Here we show through the use of distinct experimental designs that the rate of the *glmS* ribozyme reaction pathway is limited by a slow cation-dependent transition to a conformation that is capable of binding GlcN6P rapidly and stimulating self-cleavage (Figure 7). Formation of this structure in the absence of GlcN6P is evidenced by data showing that this conformational step can be accomplished during a prefolding step in which the RNA is incubated in divalent cations or high concentrations of monovalent cations (Figure 2; K. M. Brooks and K. J. Hampel, unpublished data). Addition of GlcN6P to this prefolded RNA results in very fast catalysis [72 min^{-1} (Figure 2)]. Previous reports of the *glmS* ribozyme cleavage rate have generally used experimental designs in which this slow conformational step is likely to limit the reaction rate, and they report RNA cleavage rates similar to our results from complex-initiated reactions, in the range of 3−6 min^{-1} (*7*, *9*, *12*, *13*, *15*). In these previous reports, reactions were initiated by the addition of divalent cations to the *glmS* mRNA or by mixing the two RNA components that are required to interact in trans to form the reactive RNA structure. Thus, both designs require that the *glmS* ribozyme fold into its active conformation during the experimental time course and therefore must encounter this slow step. One exception in the literature is a report in which self-cleaving

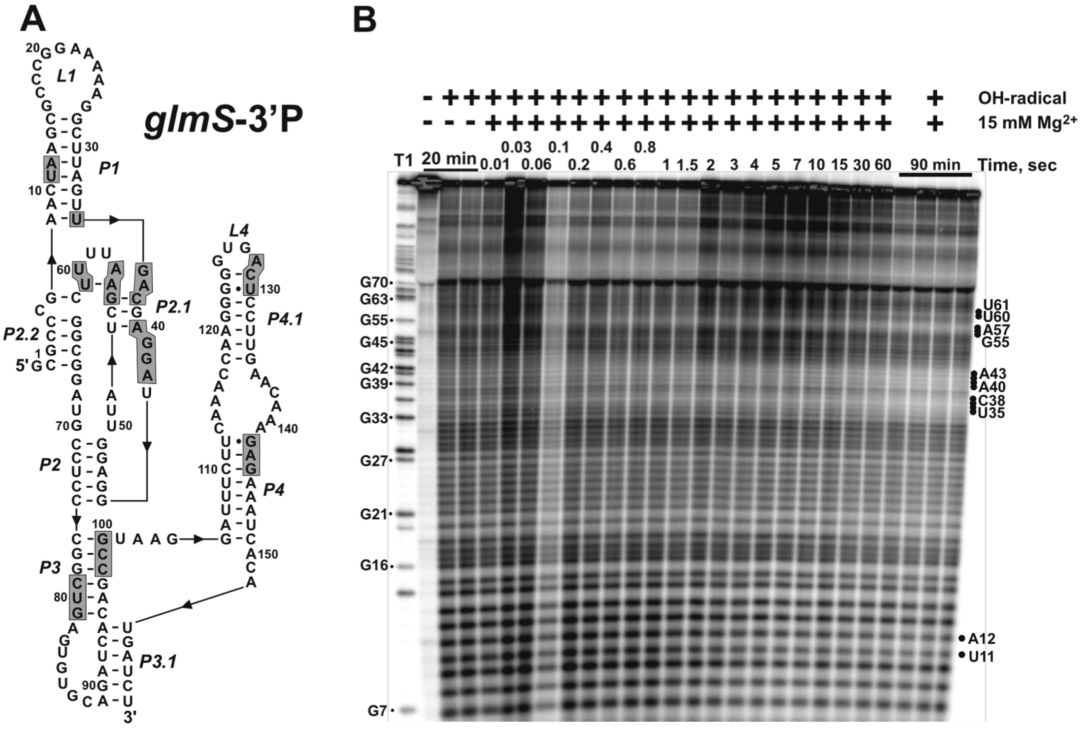

FIGURE 4: Folding kinetics determined by time-resolved hydroxyl-radical footprinting of 5′-end-labeled *glmS*-3′P. (A) Secondary structure of the 3′P of self-cleavage activity (*glmS*-3′P) used for these experiments. Sites of protection quantified in this study are shaded gray. (B) Typical gel arrangement of samples and results. The RNA was allowed to fold for the time indicated at 25 °C in a buffer containing 15 mM GlcN6P in the presence or absence of 15 mM Mg^{2+} and then treated with hydroxyl-radical generating reagents as described in Materials and Methods. Reaction products were separated on a 15% (w/v) acrylamide, 8 M urea gel and imaged on a Bio-Rad phosphorimager. Black circles denote sites that are protected by global tertiary structure formation and are quantifiable from this gel, and their nucleotide positions are indicated to the right of the gel. An RNase T1 digestion ladder to the left of the experimental lanes was used in conjunction with background hydroxyl-radical cleavage to identify protected residues.

glmS RNA was mixed with a Mg^{2+}-containing buffer for 1 min prior to addition of GlcN6P (*20*). These reactions followed a strongly biphasic reaction coordinate where there was an initial burst of activity that accounted for less than half the magnitude of the self-cleavage reaction with a rate of 15 min^{-1} followed by a slower rate (1 min^{-1}) accounting for the remaining reaction amplitude. We observed a similar reaction coordinate in our experiments using a cation-initiated reaction with the *glmS*-Rz−S complex (Figure 2C). In light of the data reported here, an alternative interpretation of these data is that the short preincubation in folding buffer allowed a fraction of the molecules to fold and subsequently react in the rapid burst upon incubation with ligand. The remaining molecules reacted after completing the rate-limiting conformational step.

It is important to note that our only rate data for this slow folding step come from experiments in which the catalytic RNA is folded in the presence of GlcN6P during cleavage reactions. Therefore, we do not have data for the influence of GlcN6P on the rate of this conformational change. Time-resolved footprinting experiments show rapid formation of the native tertiary structure (1 s^{-1}), without any evidence of a distinct change in structure occurring on the time scale of the slow folding step, approximately 3 min^{-1}, in the absence or presence of GlcN6P. Although our data show that the conformational change can be accomplished in the absence of ligand as described above and crystal structures show little or no difference between ligand-occupied and unbound ribozymes, we have no data regarding the influence of the ligand on the rate of this slow, rate-limiting, folding step. Therefore, we are left with the possibility that the ligand may alter the kinetics of this slow step as part of an induced-fit folding pathway. This is a difficult possibility to discard; however, there is significant evidence to support the proposal that the presence of ligand does not affect the rate of this slow step.

First, the ligand is capable of binding rapidly to the ribozyme after the RNA has undergone prefolding in Mg^{2+}. The argument would, therefore, have to be made for two distinct modes of GlcN6P binding, one to a partially formed GlcN6P binding pocket and one to a GlcN6P binding pocket that is completely formed. Second, when we plotted the reaction rate as a function of GlcN6P concentration (Figure 3 and Table 2), we found that the cleavage rates obtained using either design overlaid at GlcN6P concentrations of <0.1 mM. Under these conditions, GlcN6P binding is rate-limiting for cleavage. This suggests that the GlcN6P binding rate is the same under these conditions, and therefore, there is no functional difference between binding of GlcN6P under the two experimental designs. We would argue that this is the case because GlcN6P binding awaits formation of the same binding structure within the ribozyme core. Finally, although GlcN6P is 80% buried in the *glmS* ribozyme tertiary structure, space filling models of the ligand occupying its binding pocket clearly show that the ligand may access the binding pocket without significant accompanying conformational changes (*11*). One important interaction is the stacking of G1 above the sugar ring of GlcN6P (*11*, *12*). The exact orientation of G1 may greatly affect access to the binding pocket, and this stacking interaction may stabilize the GlcN6P binding. A more thorough analysis of the reactions rates for the two designs over this GlcN6P concentration range as a function of cation concentration, temperature, and other extrinsic factors will allow this hypothesis

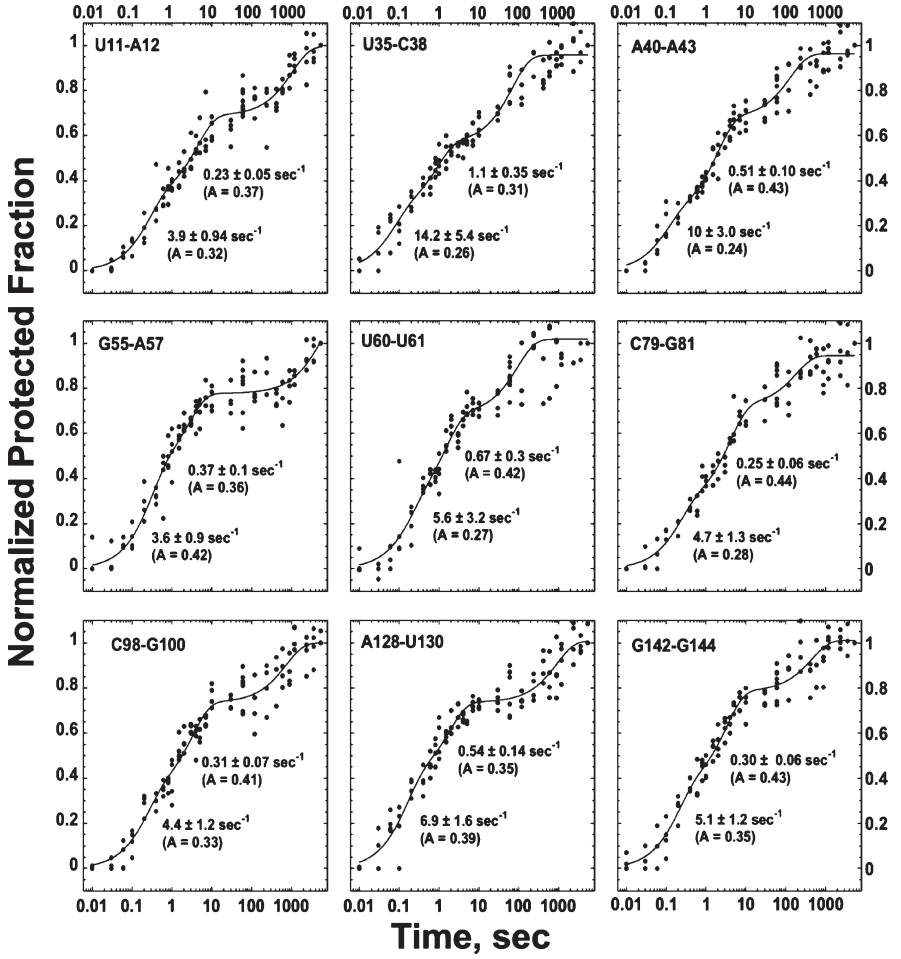

FIGURE 5: Time-resolved hydroxyl-radical footprinting of the *glmS* motif. Hydroxyl-radical protection of segments of *glmS*-3′P RNA was quantified as described in Materials and Methods, and the results of at least four independent experiments were plotted as a function of time. All data points derived from quantification of a single protected site (> 100 data points per site) were fit simultaneously to the triple-exponential equation $y = y_o + A_1(1 - e^{-t/\tau_1}) + A_2(1 - e^{-t/\tau_1}) + A_3(1 - e^{-t/\tau_1})$. The two fastest rates and their curve fit error for each site are reported along with their individual amplitude (A) calculated from the curve fit.

to be fully tested. In addition, the proposal that GlcN6P increases the rate of folding for the slow conformational change can be tested by a chase experiment in which the magnitude of a GlcN6P-initiated burst is recorded following preincubation with Mg^{2+} for different times. Guanine-sensing riboswitches are known to undergo induced-fit binding of guanine where a portion of the ligand binding pocket is preordered and upon binding of ligand an RNA flap closes over the ligand encasing it in the RNA tertiary structure (*21*, *22*). In addition, the hydroxyl-radical footprinting of the glycine riboswitch has shown partial Mg^{2+}-dependent preordering of the putative ligand binding site, a highly conserved four-helix junction, in the absence of glycine (*23*).

To gain a better understanding of the binding of the GlcN6P, we carried out a set of reactions aimed at determining the apparent binding constant of the GlcN6P under both experimental designs. Since the GlcN6P-initiated experimental design demonstrated that GlcN6P could bind rapidly to the preformed tertiary structure, we hoped that this result would enable us to better define the GlcN6P binding constant free of a rate-limiting preliminary conformational step. Our results show that the apparent K_d for GlcN6P is dramatically dependent upon the experimental design employed. The best interpretation of these data is that the maximal rate observed in GlcN6P titrations where the individual reactions are initiated by adding *glmS*-Rz and S together [complex-initiated (Figure 2A)] artificially lowers the apparent K_d for GlcN6P. This is due to the fact that the rate-limiting step in these reactions changes within the titration. At low ligand concentrations, the rate of the reaction increases with an increase in the level of GlcN6P; therefore, these reactions are limited by the rate of GlcN6P binding. When the maximal rate of the slow conformational change is approached, the reaction rate no longer increases with an increase in the level of GlcN6P, and an artificial GlcN6P saturation point is reached. In titrations where the individual reaction rates are obtained from an experimental design where the ribozyme−substrate complex is prefolded in the absence of ligand (GlcN6P-initiated), bypassing the slow step reveals a K_d closer to the intrinsic K_d for the ligand. This is because the rate at which the GlcN6P binds the ribozyme−substrate complex continues to increase with an increase in GlcN6P concentration until the rate of binding becomes saturated or a second rate-limiting step becomes apparent and the reaction rate plateaus. We have no data to argue whether this higher apparent saturation point is due to the intrinsic binding constant of GlcN6P or a new rate-limiting step.

One way in which we could find support for the proposal that the maximal rate observed in these reactions is due to the intrinsic rate of ligand binding at saturating ligand concentrations is the pH dependence of this K_d. The amino group of GlcN6P has a pK_a of 7.8. Our rate versus pH analysis does not provide strong

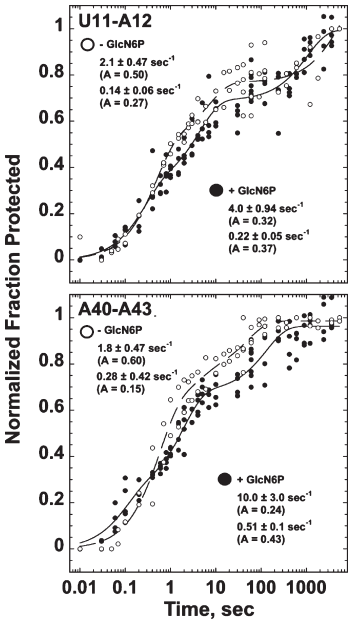

FIGURE 6: Kinetics of global tertiary folding of the *glmS* catalytic motif are unaffected by the presence of GlcN6P. Two protected sites, one due to a peripheral contact between the L4 GUGA tetraloop and its P1 receptor [U11-A12 (top panel)] and the other a result of core folding [A40-A43 (bottom panel)], were used to show the effect of GlcN6P on global folding kinetics. White and black symbols represent normalized protection amplitudes from two to four experiments in the absence and presence of GlcN6P, respectively. All data points derived from quantification of a single protected site were fit simultaneously to the triple-exponential equation $y = y_o + A_1(1 - e^{-t/\tau_1}) + A_2(1 - e^{-t/\tau_1}) + A_3(1 - e^{-t/\tau_1})$, for U11-A12 with or without GlcN6P and A40-A43 with GlcN6P, or the double-exponential equation $y = y_o + A_1(1 - e^{-t/\tau_1}) + A_2(1 - e^{-t/\tau_1})$ for A40-A43 without GlcN6P.

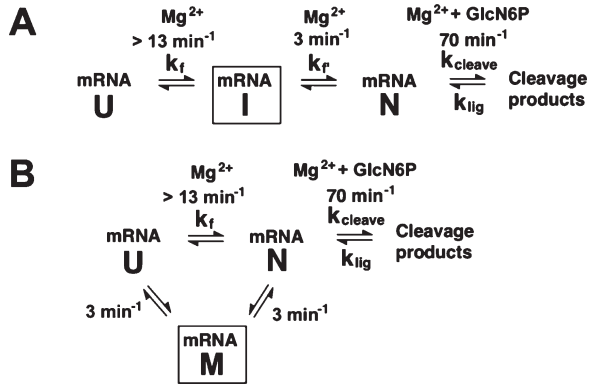

FIGURE 7: Folding and reaction pathway model for the *glmS* ribozyme that features a nativelike inactive intermediate or misfolded form. (A) Global folding from the unfolded (U) to a compact nativelike intermediate (I) structure occurs rapidly upon addition of Mg^{2+}. A second Mg^{2+}-dependent event folds the catalytic RNA into a complex capable of GlcN6P binding (N). GlcN6P binding and catalysis occur on a second time scale once the native (N) structure is formed. (B) A second possibility is that the slow folding step represents the rate of release from an off-pathway misfolded form (M) to the unfolded form (U) or to a native ligand binding form (N).

support for a model in which ionization of the amino group results in a decrease in the binding affinity for the GlcN6P, since over a 1.5 pH unit change from pH 7.5 to 6, there is a <10-fold increase in the K_d for GlcN6P. McCarthy and co-workers observed an only small, <5-fold, effect of pH on the apparent K_d for GlcN6P between pH 7.5 and 8.8 (*13*). This is in contrast to data from the *Bacillus anthracis* trans cleavage system where a 100-fold decrease in the K_m for GlcN6P was observed as the pH was increased from 6 to 7.5 (*12*). Further biochemical analysis with GlcN6P and coenzyme analogues with altered amino pK_a values will need to be conducted to determine if this change in K_d is determined by ionization of the amino group of the ligand.

Riboswitches control gene expression primarily at the level of transcription by altering the level of premature transcriptional termination or at the point of translation initiation by controlling access of the ribosome to the mRNA (*5*, *24*). The *glmS* riboswitch exhibits genetic control at the level of mRNA stability where GlcN6P-induced self-cleavage is the first committed step in the mRNA degradation pathway (*7*, *8*). Our data suggest that the speed of operation of the RNA cleavage switch will be responsive to a wide range of GlcN6P concentrations for mRNAs that have transited through the rate-limiting step in the reaction pathway. It will be interesting to determine the range over which GlcN6P is regulated in vivo to put our data into a physiological context. The very high K_d for GlcN6P is unusual for riboswitches and may be related to the relative abundance of this metabolite and the range of concentration over which it needs to be regulated in vivo.

Our results provide a method by which to study *glmS* ribozyme catalysis in the absence of this slow step. GlcN6P is capable of rapidly binding to the preformed catalytic pocket. Furthermore, when the cleavage rate is plotted against the GlcN6P concentration for both designs and overlaid, we find that the rates are the same when the concentration of the GlcN6P becomes limiting for catalysis (Figure 3C).

The slow rate-limiting folding step observed in cleavage kinetics experiments led us to determine the rate of folding of the global tertiary structure as defined by time-resolved hydroxyl-radical footprinting. Our previous work has shown extensive solvent protection throughout the *glmS* riboswitch that was not dependent on the presence of GlcN6P. We were surprised to find that the rate of formation for the solvent-protected tertiary structure does not mimic the kinetics of Mg^{2+}-induced catalysis, but is much more rapid (Figures 4 and 5). We were able to fit our data to a triple-exponential equation giving three distinct folding rates and amplitudes for each protected site. The fastest rates for solvent protection in our experiments range from 3.6 s^{-1} for positions G55−A57 to 14.2 s^{-1} for a string of highly conserved core residues, U35−C38. It should be noted that the solvent protections that arise from the interaction between the L4 tetraloop and its receptor in P1, A128−U130 and U11-A12, respectively, have folding rates that differ by almost 2-fold. Theoretically, these two rates should be equal. This underscores the importance of being cautious about interpreting differences in folding rates within the range we have observed with *glmS*-3′P. Our best interpretation of the data we have obtained is that it is consistent with a concerted folding of the ribozyme to a nativelike structure. Concerted folding of a large ribozyme had been previously observed for the yeast group II intron, aI5γ. This intron folds in a manner that appears concerted due to the presence of a slow rate-limiting step in the folding pathway (*25*−*27*). The group I intron from the bacterium *Azoarcus* has been shown to undergo rapid folding ($\sim$10 s^{-1}), where all solvent-protected sites become folded at similar rates (*28*). Finally, the *Neurospora* Varkud satellite ribozyme has been shown to fold into its solvent-protected tertiary structure very rapidly, with all sites reaching a maximum level of protection within 2 s (*29*). Our data similarly argue that large highly structured RNAs are capable of forming complex "nativelike" conformations during

a rapid cation-dependent compaction. A third slow folding folding phase is not well-defined in our experiments and does not clearly coincide with the slow cation- or complex-initiated cleavage rates (Figure 2). Thus, we have no evidence to argue that this slow folding could be the rate-limiting step that we observed during these catalytic assays. In addition, we have observed that the *glmS*-cis construct is quite well behaved kinetically, with a very large fraction (0.86) of molecules cleaving in the first exponential phase (Figure 2B and Table 1). This suggests to us that folding of a significant population of the *glmS*-3′P molecules may be uniquely perturbed by an initial folding trap. The *glmS*-3′P molecule is missing a 39-nucleotide stretch of RNA present in the uncleaved precursor, and this section of the mRNA contains several residues conserved among the *glmS* riboswitches (*7*). It is possible that this region gives rise to more homogeneous cation-dependent folding.

Our previous work that defined the solvent-inaccessible core of the ribozyme demonstrated that GlcN6P does not influence the final pattern or amplitude of solvent protection (*10*). To follow up on these experiments and to expand our understanding of the global folding requirements, we performed time-resolved hydroxyl-radical footprinting experiments in the presence and absence of GlcN6P (Figure 6). We observed a small increase in the tertiary folding rate in the presence of GlcN6P (2−5-fold) for the fastest folding rates. This is not, however, an increase sufficiently large in rate to make a clear argument that the ligand increases the rate of folding. We were, therefore, unable to identify a role for the ligand in the folding kinetics of the riboswitch.

Our time-resolved footprinting data indicate that in vitro the *glmS* ribozyme undergoes rapid (0.23−14.2 s^{-1}) tertiary folding from the secondary structure to a tertiary structure with the native ribozyme L4 tetraloop−P1 stem interaction and significant solvent protection of the conserved ribozyme core. Therefore, many features of the native ribozyme structure appear rapidly upon incubation in Mg^{2+}-containing solutions in vitro. When catalysis is initiated by the addition of Mg^{2+} to the RNA, incubated with GlcN6P, the cleavage reaction rate is at least 5-fold slower and is not limited by the rate of GlcN6P binding or chemical catalysis as indicated by experiments designed to isolate these steps from preliminary folding steps. One possibility is that rapid global folding gives rise to an intermediate which folds slowly to a native structure capable of rapid GlcN6P binding (Figure 7A). This intermediate retains significant native structure as revealed by hydroxyl-radical footprinting. A second possibility is that this slow step represents the rate of escape from a misfolded, off-pathway structure. Such a misfolded form would retain many elements of the native *glmS* ribozyme structure, including the L4 tetraloop−P1 receptor interaction as evidenced by time-resolved footprinting analysis (Figure 5). Such misfolding, or non-fast track folding, is not without precedent. The *Tetrahymena* group I intron folds into a compact structure with a significant native and non-native structure (*30*, *31*). We have no direct evidence that places the *glmS* system into one of these categories, but the question is very interesting and can be addressed by the methods utilized for other large catalytic RNAs.

ACKNOWLEDGMENT

We thank Dr. John M. Burke for generously supporting this independent line of research and Joyce Heckman, Ethan Guth, Christopher Francklyn, and Iwona Buskiewicz for providing helpful discussions.

SUPPORTING INFORMATION AVAILABLE

Plots of cleavage rate, k_{obs}, versus the concentration of GlcN6P at five different pHs demonstrate that complex-initiated and GlcN6P-initiated reactions yield similar rates at ligand concentrations of < 0.5 mM. This material is available free of charge via the Internet at http://pubs.acs.org.

REFERENCES

(1) Winkler, W., Nahvi, A., and Breaker, R. R. (2002) Thiamine derivatives bind messenger RNAs directly to regulate bacterial gene expression. *Nature 419*, 952–956.
(2) Mironov, A. S., Gusarov, I., Rafikov, R., Lopez, L. E., Shatalin, K., Kreneva, R. A., Perumov, D. A., and Nudler, E. (2002) Sensing small molecules by nascent RNA: A mechanism to control transcription in bacteria. *Cell 111*, 747–756.
(3) Nudler, E., and Mironov, A. S. (2004) The riboswitch control of bacterial metabolism. *Trends Biochem. Sci. 29*, 11–17.
(4) Barrick, J. E., Corbino, K. A., Winkler, W. C., Nahvi, A., Mandal, M., Collins, J., Lee, M., Roth, A., Sudarsan, N., Jona, I., Wickiser, J. K., and Breaker, R. R. (2004) New RNA motifs suggest an expanded scope for riboswitches in bacterial genetic control. *Proc. Natl. Acad. Sci. U.S.A. 101*, 6421–6426.
(5) Winkler, W. C., and Breaker, R. R. (2005) Regulation of bacterial gene expression by riboswitches. *Annu. Rev. Microbiol. 59*, 487–517.
(6) Kobayashi, K., Ehrlich, S. D., Albertini, A., Amati, G., Andersen, K. K., Arnaud, M., Asai, K., Ashikaga, S., Aymerich, S., Bessieres, P., Boland, F., Brignell, S. C., Bron, S., Bunai, K., Chapuis, J., Christiansen, L. C., Danchin, A., Debarbouille, M., Dervyn, E., Deuerling, E., Devine, K., Devine, S. K., Dreesen, O., Errington, J., Fillinger, S., Foster, S. J., Fujita, Y., Galizzi, A., Gardan, R., Eschevins, C., Fukushima, T., Haga, K., Harwood, C. R., Hecker, M., Hosoya, D., Hullo, M. F., Kakeshita, H., Karamata, D., Kasahara, Y., Kawamura, F., Koga, K., Koski, P., Kuwana, R., Imamura, D., Ishimaru, M., Ishikawa, S., Ishio, I., Le Coq, D., Masson, A., Mauel, C., Meima, R., Mellado, R. P., Moir, A., Moriya, S., Nagakawa, E., Nanamiya, H., Nakai, S., Nygaard, P., Ogura, M., Ohanan, T., O'Reilly, M., O'Rourke, M., Pragai, Z., Pooley, H. M., Rapoport, G., Rawlins, J. P., Rivas, L. A., Rivolta, C., Sadaie, A., Sadaie, Y., Sarvas, M., Sato, T., Saxild, H. H., Scanlan, E., Schumann, W., Seegers, J. F., Sekiguchi, J., Sekowska, A., Seror, S. J., Simon, M., Stragier, P., Studer, R., Takamatsu, H., Tanaka, T., Takeuchi, M., Thomaides, H. B., Vagner, V., van Dijl, J. M., Watabe, K., Wipat, A., Yamamoto, H., Yamamoto, M., Yamamoto, Y., Yamane, K., Yata, K., Yoshida, K., Yoshikawa, H., Zuber, U., and Ogasawara, N. (2003) Essential *Bacillus subtilis* genes. *Proc. Natl. Acad. Sci. U.S.A. 100*, 4678–4683.
(7) Winkler, W. C., Nahvi, A., Roth, A., Collins, J. A., and Breaker, R. R. (2004) Control of gene expression by a natural metabolite-responsive ribozyme. *Nature 428*, 281–286.
(8) Collins, J. A., Irnov, I., Baker, S., and Winkler, W. C. (2007) Mechanism of mRNA destabilization by the *glmS* ribozyme. *Genes Dev. 21*, 3356–3368.
(9) Tinsley, R. A., Furchak, J. R., and Walter, N. G. (2007) Trans-acting *glmS* catalytic riboswitch: Locked and loaded. *RNA 13*, 468–477.
(10) Hampel, K. J., and Tinsley, M. M. (2006) Evidence for preorganization of the *glmS* ribozyme ligand binding pocket. *Biochemistry 45*, 7861–7871.
(11) Klein, D. J., and Ferré-D'Amaré, A. R. (2006) Structural basis of *glmS* ribozyme activation by glucosamine-6-phosphate. *Science 313*, 1752–1756.
(12) Cochrane, J. C., Lipchock, S. V., and Strobel, S. A. (2007) Structural investigation of the *glmS* ribozyme bound to Its catalytic cofactor. *Chem. Biol. 14*, 97–105.
(13) McCarthy, T. J., Plog, M. A., Floy, S. A., Jansen, J. A., Soukup, J. K., and Soukup, G. A. (2005) Ligand requirements for *glmS* ribozyme self-cleavage. *Chem. Biol. 12*, 1221–1226.
(14) Jansen, J. A., McCarthy, T. J., Soukup, G. A., and Soukup, J. K. (2006) Backbone and nucleobase contacts to glucosamine-6-phosphate in the glmS ribozyme. *Nat. Struct. Mol. Biol. 13*, 517–523.
(15) Walter, N. G., Yang, N., and Burke, J. M. (2000) Probing non-selective cation binding in the hairpin ribozyme with Tb(III). *J. Mol. Biol. 298*, 539–555.
(16) Chowrira, B. M., Berzal-Herranz, A., and Burke, J. M. (1993) Novel RNA polymerization reaction catalyzed by a group I ribozyme. *EMBO J. 12*, 3599–3605.

(17) Shcherbakova, I., and Brenowitz, M. (2008) Monitoring structural changes in nucleic acids with single residue spatial and millisecond time resolution by quantitative hydroxyl radical footprinting. *Nat. Protoc. 3*, 288–302.
(18) Hampel, K. J., and Burke, J. M. (2001) A conformational change in the "loop E-like" motif of the hairpin ribozyme is coincidental with domain docking and is essential for catalysis. *Biochemistry 40*, 3723–3729.
(19) Klein, D. J., Been, M. D., and Ferré-D'Amaré, A. R. (2007) Essential role of an active-site guanine in *glmS* ribozyme catalysis. *J. Am. Chem. Soc. 129*, 14858–14859.
(20) Wilkinson, S. R., and Been, M. D. (2005) A pseudoknot in the 3′ non-core region of the *glmS* ribozyme enhances self-cleavage activity. *RNA 11*, 1788–1794.
(21) Ottink, O. M., Rampersad, S. M., Tessari, M., Zaman, G. J., Heus, H. A., and Wijmenga, S. S. (2007) Ligand-induced folding of the guanine-sensing riboswitch is controlled by a combined predetermined induced fit mechanism. *RNA 13*, 2202–2212.
(22) Noeske, J., Buck, J., Furtig, B., Nasiri, H. R., Schwalbe, H., and Wohnert, J. (2007) Interplay of 'induced fit' and preorganization in the ligand induced folding of the aptamer domain of the guanine binding riboswitch. *Nucleic Acids Res. 35*, 572–583.
(23) Lipfert, J., Das, R., Chu, V. B., Kudaravalli, M., Boyd, N., Herschlag, D., and Doniach, S. (2007) Structural transitions and thermodynamics of a glycine-dependent riboswitch from *Vibrio cholerae*. *J. Mol. Biol. 365*, 1393–1406.
(24) Barrick, J. E., and Breaker, R. R. (2007) The distributions, mechanisms, and structures of metabolite-binding riboswitches. *Genome Biol. 8*, R239.
(25) Swisher, J. F., Su, L. J., Brenowitz, M., Anderson, V. E., and Pyle, A. M. (2002) Productive folding to the native state by a group II intron ribozyme. *J. Mol. Biol. 315*, 297–310.
(26) Su, L. J., Brenowitz, M., and Pyle, A. M. (2003) An alternative route for the folding of large RNAs: Apparent two-state folding by a group II intron ribozyme. *J. Mol. Biol. 334*, 639–652.
(27) Fedorova, O., Waldsich, C., and Pyle, A. M. (2007) Group II intron folding under near-physiological conditions: Collapsing to the near-native state. *J. Mol. Biol. 366*, 1099–1114.
(28) Rangan, P., Masquida, B., Westhof, E., and Woodson, S. A. (2003) Assembly of core helices and rapid tertiary folding of a small bacterial group I ribozyme. *Proc. Natl. Acad. Sci. U.S.A. 100*, 1574–1579.
(29) Hiley, S. L., and Collins, R. A. (2001) Rapid formation of a solvent-inaccessible core in the *Neurospora* Varkud satellite ribozyme. *EMBO J. 20*, 5461–5469.
(30) Kwok, L. W., Shcherbakova, I., Lamb, J. S., Park, H. Y., Andresen, K., Smith, H., Brenowitz, M., and Pollack, L. (2006) Concordant exploration of the kinetics of RNA folding from global and local perspectives. *J. Mol. Biol. 355*, 282–289.
(31) Russell, R., Das, R., Suh, H., Travers, K. J., Laederach, A., Engelhardt, M. A., and Herschlag, D. (2006) The paradoxical behavior of a highly structured misfolded intermediate in RNA folding. *J. Mol. Biol. 363*, 531–544.